4
Solution Processed Hafnia Nanoaggregates: Influence of Surface Oxygen on Catalytic Soot Oxidation

The work described in this chapter has been published in *ACS Sustainable Chem. Eng. 2018, 6, 11286−11294*.

The process of Hafnium dioxide (HfO_2) nanoaggregates are synthesized by sol−gel and hydrothermal routes followed by hydrogen annealing at different time durations. The proposed study aims to explore the effect of hydrogen annealing time on the properties of HfO_2 and also envisage the catalytic soot oxidation using HfO_2 nanoaggregates. It is observed that annealing under a hydrogen atmosphere brought about substantial changes in certain attributes such as chemical and textural properties with marginal changes in some other properties like optical activity and bandgap. The pristine HfO_2 without hydrogen annealing showed a lower ignition temperature. In contrast, hydrogen annealed HfO_2 for 2h showed the best catalytic performance characterized by the soot combustion temperature (T_{50}) in contrast to samples prepared at a longer duration because of the higher surface adsorbed oxygen species in its widely distributed pores.

4.1 Experimental section

4.1.1 Synthesis of HfO_2 Nanoparticles

HfO_2 and H-HfO_2 nanospheres were prepared via a modified sol−gel process followed by hydrothermal treatment.(Laishram, Shejale et al. 2016) Hafnium isopropoxide (HIP) (40 mM) was added dropwise into a mixture of 200 mL of ethanol and 1.975 g of hexadecylamine (HDA) under vigorous stirring. The mixture was kept in the dark for 18 h and then filtered. The filtered white precipitate was dried under air at room temperature and crushed to get a fine powder. The crushed powder (0.8 g) is dispersed in 10 mL of ethanol, 5 mL of deionized water (DI), and 0.25 mL of liquor ammonia by ultrasonication for 10 min. The mixture is then transferred to a Teflon-lined steel autoclave and kept for 8 h at 160 °C in a preheated oven. After the completion of the reaction, the resultant product was filtered and washed repeatedly with DI water followed by absolute ethanol before drying in a vacuum oven at 70 °C overnight. The obtained sample was subsequently ground in a mortar pestle and annealed in a tubular furnace at 500 °C for 2 h in the air to obtain a white colored pristine HfO_2 (p-HfO_2). Similarly, samples were annealed for different time intervals at 2, 6, and 10 h under a gas flow of 10% H_2 and 90% N_2 for 500 °C at a heating rate of 2.5 °C min^{-1} to get off-white colored H-HfO_2 nanoaggregates. The HfO_2 solid nanosphere aggregates were prepared by a combination of sol-gel and hydrothermal processes. In the foremost sol-gel step, HfO_2 precursor beads were prepared by mixing the HfO_2 precursor with hexadecylamine (HDA) in an alcoholic solution. The interaction between the hydrolyzed HIP molecules and the amine group of HDA results in the formation of organic-inorganic oligomers with HDA acting as a structure directing agent. These oligomers polymerize, condense, and precipitate, leading to the formation of HfO_2 precursor beads. These precursor beads undergo a hydrothermal treatment in the next step to give nanoaggregates of HfO_2. Finally, the powdered nanoaggregates are annealed at 500 °C in air for 2 h resulting in HfO_2 nanoaggregates referred to as p-HfO_2, and these were hydrogenated by annealing under H_2 at 500 °C for different time intervals (2, 6, and 10 h) and designated as H-HfO_2_2h, H-HfO_2_6h, and H-HfO_2_10h, respectively. A schematic illustration of the synthesis process is given in Figure 4.1a.

Figure 4.1: (a) Schematic demonstrating the synthesis of HfO_2 solid nanosphere aggregates by sol–gel and hydrothermal methods. (b) Representation of the process of soot-catalyst preparation for soot oxidation activity in a TGA crucible.

4.1.2 Soot Oxidation Activity

Catalytic soot oxidation activity was measured by thermogravimetric (TGA) analysis in a PerkinElmer, Simultaneous Thermal Analyzer (STA) equipped with a digital temperature controller from PolyScience. The model soot used for this study was carbon black (acetylene black) obtained from Alfa Aesar (1333-86-4). The weight loss measurement of the catalyst/soot mixture at a 4:1 ratio was studied in the temperature range from 30 to 900 °C under zero air at a 10 °C/min heating rate with an air-flow rate of 20 mL/min. The contact between the catalyst and soot plays a vital role, and the catalytic activity depends strongly on the interaction between the two solids and air. Tight contacts have been maintained by grinding the soot and catalyst in a mortar; this is important for the transfer of active oxygen with a catalyst surface and soot particles. Figure 4.1b represents the schematic for the measurement of soot oxidation activity.

4.2 Results and discussion

4.2.1 Structural Analysis

The XRD patterns of pristine and hydrogen annealed HfO_2 nanoaggregates are shown in Figure 4.2a; the patterns correspond to the monoclinic phase of HfO_2, and all of the peaks are identified and indexed accordingly as per JCPDS data card no. 034−0104. Further, no other secondary peaks were observed, indicating that the as synthesized HfO_2 is of pure phase. The most prominent peak of HfO_2 matches the $(\bar{1}\bar{1}1)$ monoclinic phase of HfO_2, which is evident at 2θ equal to 28.2°. (Ramana, Bharathi et al. 2012) H-HfO_2 showed a successive increase in peak intensity, with a 2θ shift toward a lower angle corresponding to higher d-spacing (Figure 4.2b). Additionally, an increase in average crystallite size can be observed as a result of hydrogen gulping by HfO_2 particles upon annealing for a higher duration (2 h < 6 h < 10 h) as shown in Figure 4.2c. It was also found that the observed peak intensity is highest for H-HfO_2_2h and decreases with an increase in annealing time, which might be because of texturing in the crystal lattice. Furthermore, it was observed that the particle size (calculated from the Williamson Hall method) and the lattice strain increases with an increase in annealing time under an H_2 atmosphere and is highest for H HfO_2_10h nanoaggregates (Table 4.1, Figure 4.2d). The strain states increase as HfO_2_2h < p-HfO_2 < H-HfO_2_2h < H-HfO_2_6h < H-HfO_2_10h. This is a consequence of prolonged annealing under reduced ambience, leading to the introduction of H_2 in the lattice of HfO_2, which creates structural defects and oxygen vacancies in higher concentration.(Hosseinpour, Yung et al. 2014) Thus, the increased lattice strain (Figure 4.2d) for

hydrogen annealed HfO_2 nanoaggregates is a result of the increase in the grain boundaries and defects present. Annealing under reduced atmosphere imposes strain upon the Hf lattice, which affects the oxygen vacancy formation and surface chemical activity of the synthesized HfO_2 nanoaggregates. Thus, the increase in lattice strain is likely to affect the adsorption capability and binding ability of the adsorbates strongly. The effect of strain upon the synthesized HfO_2 nanoaggregates was determined by means of a Williamson Hall plot Figure 4.2(e, f, g and h)).

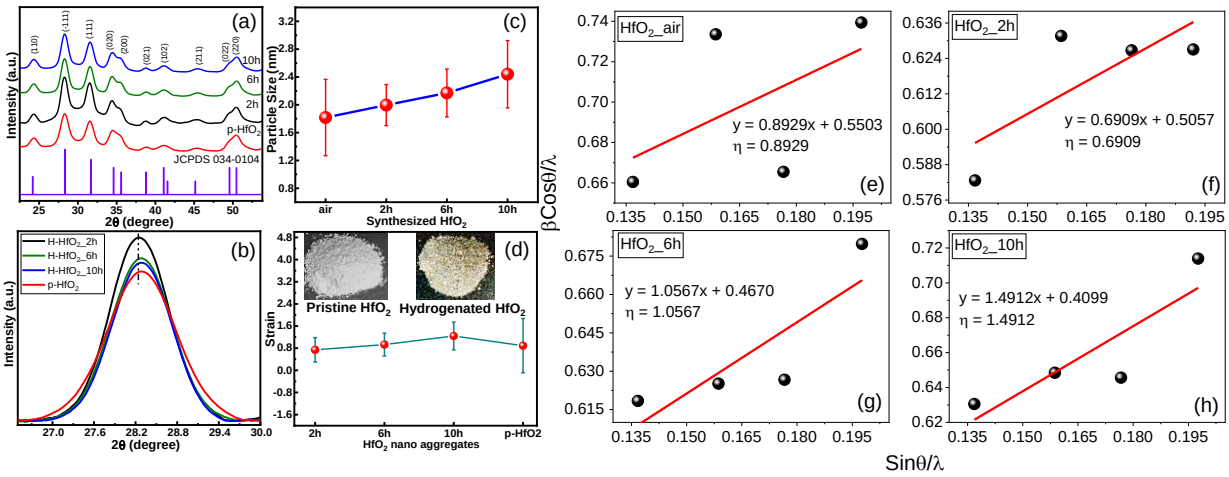

Figure 4.2: (a) XRD patterns of p-HfO_2 nanoparticles annealed in air and H-HfO_2_2h, H-HfO_2_6h, and H-HfO_2_10h, (b) Plot showing peak intensity against with a 2θ shift, (c) Plot showing variation in particle size of the synthesized HfO_2 nanoaggregates, (d) variation of strain calculated from Williamson Hall plot and inset is the difference in color of p-HfO_2 showing white color and H-HfO_2 with off-white color after annealing in H_2 and (e, f, g and h) Williamson Hall plot of the synthesised HfO_2 nano aggregates, the strain is found from the slope and the crystallite size from the y-intercept by the linear fitting.

Table 4.1. Particle size, *d*-spacing and strain calculated for the hydrogenated HfO_2.

Sl. No.	*Sample*	*Particle Size (nm)*	*d-spacing (Å)*	*Strain (%)*
1.	p-HfO_2	1.82	3.15	0.89
2.	H-HfO_2_2h	2.00	3.15	0.69
3.	H-HfO_2_6h	2.17	3.15	1.05
4.	H-HfO_2_10h	2.44	3.15	1.49

A plot of catalytic activity and strain for all the synthesized nanoaggregates is given in Figure 4.5e. Chaubey et al. report poor crystallization of HfO_2 nanoparticles under a reducing atmosphere (10% H_2 in N_2) at 500 °C temperature for 4h. (Chaubey, Yao et al. 2012) Contrarily, the synthesized HfO_2 showed uniform crystallinity for the entire annealing time range from 2 to 10 h under a reducing atmosphere. However, it is interesting to observe the decrease in crystallite size for all of the hydrogen annealed HfO_2 compared to the air annealed pristine p-HfO_2 (Figure 4.2c and Table 4.1).

4.2.2 Textural Analysis: TEM Analysis

TEM images show nanoaggregates of ~50-100 nm consisting of loosely bound nanoparticles (~5-10 nm) resembling a bunch of grapes. The size observed under TEM is different from that calculated from XRD probably because of the aggregated nature of nanoparticles.(Uvarov and Popov 2013) As observed from the TEM images in Figure 4.3a, b and c, the interparticle pore widening takes place upon hydrogen annealing. The average size of the HfO_2 aggregate, as well as nanoparticles visibly increase upon successively increasing hydrogen annealing from 2 to 6 h. As seen from HRTEM images, interplanar spacing is well-resolved for some of the non-overlapping nanoparticles because of expansion of the aggregated structure upon hydrogenation as seen for 6h_hydrogen annealed HfO_2 in Figure 4.3f. Also, disordering of the crystal lattice as indicated by the encircled dotted lines is observed because of the introduction of hydrogen into the HfO_2 lattice (Figure 4.3e, f) as compared to the pristine case

(Figure 4.3d). The $(1\bar{1}1)$ oriented HfO_2 nanoparticles (d ≈ 0.31 nm) corresponding to the monoclinic phase could be easily identified in the HRTEM images as well. Also, the sharp dotted rings of the SAED (selected area electron diffraction) pattern (Figure 4.3g-i) indicate that the polycrystalline and disordered nature of HfO_2 increases upon H_2 annealing.

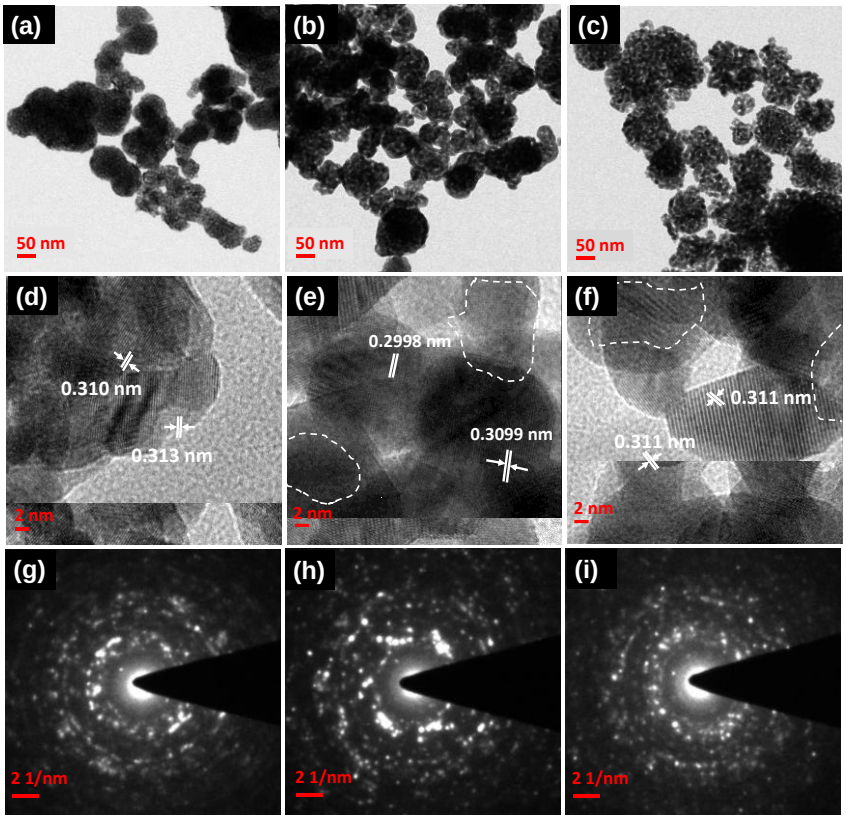

Figure 4.3: (a) TEM and HRTEM images of air annealed HfO_2 (a, d), 2 h (b, e), and 6 h (c, f) hydrogen annealed HfO_2. The SAED patterns of air annealed (g) and hydrogen annealed 2h (h) and 6h (i) samples, respectively, indicating the polycrystalline nature of HfO_2.

4.2.3 Textural Analysis: BET Analysis

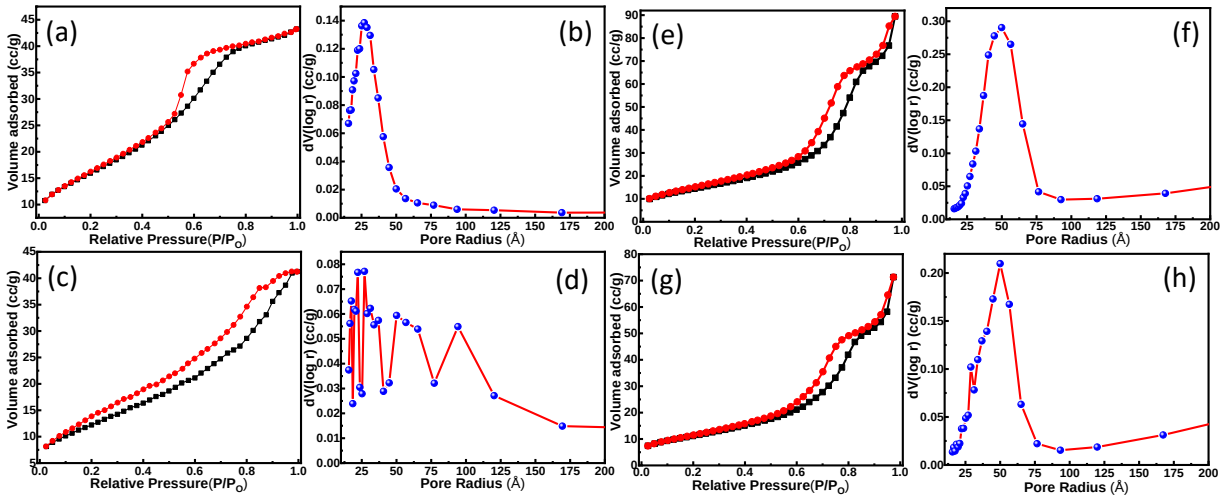

Figure 4.4: (a) BET adsorption-desorption isotherm and pore size desorption curve for p-HfO_2 (a, b), H-HfO_2_2h (c, d), H-HfO_2_6h (e, f), and HHfO_2_10h (g, h), respectively.

To further understand the nature and geometry of the pores formed, BET adsorption–desorption isotherms were studied and analysed for the as-synthesized p-HfO_2, H-HfO_2_2h, H-HfO_2_6h, and H-HfO_2_10h nanoparticles. The presence of the broad and wide hysteresis loop with a delay in the condensation-evaporation process is due to the porous nature of the material. The adsorption curves show an early initial monolayer coverage

followed by multilayer formation as observed in Figure 4 for all of the synthesized nanomaterials. The p-HfO_2 (Figure 4.4a) suggests the existence of the "ink bottleneck" type of pores following H_2 hysteresis of the IUPAC classification.(Lowell, Shields et al. 2004, Grosman and Ortega 2008, Nguyen, Fan et al. 2013, M. V. Raja and Barron 2019) The adsorption isotherm increases gradually until a relative P/P_0 of 0.6 followed by a change in slope at the curve beyond 0.6, which is attributable to the condensation taking place at the neck and the interconnected inner-bottled structure, respectively. However, the desorption curve of this isotherm tracked a delayed curve during the evaporation process up to 0.6 P/P_0 and beyond 0.6 of the neck and inner bottle correspondingly. The delay in such a case might be the effect of pore-blocking because of the presence of the interconnected network of the ink bottleneck-like pore structures. The pore size distribution calculated from the BJH desorption curve and was found to be ~0.054 cc/g with a pore radius of ~2.5 nm as shown in Figure 4.4b.

Table 4.2: Surface properties of HfO_2 air, 2h, 6h and 10h from BET analysis.

Sl. No.	*Sample Name*	*Surface Area (m^2/g)*	*Pore Volume (cc/g)*	*Pore Radius (Å)*
1.	p-HfO_2	57.81	0.05	25.22
2.	H-HfO_2_2h	44.95	0.05	17.50
3.	H-HfO_2_6h	51.76	0.47	44.59
4.	H-HfO_2_10h	40.88	0.67	49.99

Also, the hysteresis loop for p-HfO_2 Figure 4.4a is associated with a type-IV isotherm indicating capillary condensation in mesopores with a surface area of 57.81 m^2/g. The hydrogen annealed H-HfO_2_2h nanoparticles, unlike p-HfO_2, followed a type-III BET isotherm with a mixed type H2+H3 hysteresis loop as shown in Figure 4.4c.(Sing and Williams 2004, Nayak and Nayak 2016) It signals that the unrestricted multilayer formation as the lateral interaction between the absorbed molecules show stronger interaction compared to the adsorbate and the adsorbent surface. Additionally, it can be inferred that the pores, in this case, have a narrow (~1.5 nm radius) bottleneck type of pores along with plate-like lamellar aggregates forming slit porous nanostructures. The BJH pore size distribution is rather broad with pore sizes ranging from 1.5 to 17 nm with no definite maxima (Figure 4.4d). A slight decrease in pore volume (0.052 cc/g) was observed with a surface area of 44.95 m^2/g. This also agrees well with the observed changes in the TEM images in Figure 4.3b, c. As the annealing temperature increases to 6 and 10 h, the type of isotherms starts to conform to a similar type-V isotherm following H3 hysteresis behaviour as given in Figure 4.4e, g. The pore radius at this point increases to 4.4 and 4.9 nm for HHfO_2_6h and H-HfO_2_10h, respectively, as shown in Figure 4.4f, h. The detail pore size and surface area values were evaluated and are presented in Table 4.2. The increase in pore radius indicates swelling of particles as observed virtually under the TEM (Figure 4.3c). Similar observations can be made in XRD, where the strain % increases with an increase in annealing time. The type-V isotherm at higher P/P_0 is associated with molecular clustering, and pore filling observed in microporous and mesoporous adsorbents. In this work, BJH analysis is used for the determination of pore size. Since, N_2 is used as the adsorbate with a cross-sectional area of 16.2 $Å^2$/ molecule, BJH analysis is valid for mesopores with pore sizes between 2 and 50 nm. The pore size for pristine HfO_2 is slightly less than 2 nm and becomes ~4.9 nm upon hydrogen annealing for 10 h.

4.2.4 Chemical Analysis: XPS Analysis

To study the chemical bonding of the synthesized HfO_2 and the effect of different annealing atmosphere, XPS analysis was performed. HfO_2 being highly insulating in nature showed a charging effect and hence a shift in the peak toward higher binding energy. The Hf 4f spectra for p-HfO_2 and hydrogenated-HfO_2 were fitted to three and four curves, respectively, corresponding to Hf $4f_{7/2}$ and Hf $4f_{5/2}$ peak levels for dioxides and suboxides (Figure 4.5a, b). The peak area ratios of j = 5/2 and j = 7/2 were kept at 1.4, and the binding energy difference

value of 1.7 eV was kept constant. The observed peaks have a large width (>0.9 eV) and hence can be assigned to suboxide and completely oxidized Hf^{4+} (Table 4.3). The major peaks for p-HfO_2 and H-HfO_2 at 16.99 and 16.64 eV correspond to Hf $4f_{7/2}$, and the shoulder peak at 18.65 and 18.19 eV corresponds to Hf $4f_{5/2}$.

Table 4.3. Binding Energy of O 1s and Hf 4f Core Levels for p-HfO_2 and H-HfO_2.

Signal	*p-HfO_2*		*H-HfO_2*	
	B.E. (eV)	*FWHM (eV)*	*B.E. (eV)*	*FWHM (eV)*
$O_{\alpha 2}$	532.8	1.6	532.4	1.6
$O_{\alpha 1}$	530.5	2.5	529.8	2.9
O_{β}	529.0	6.3	526.3	3.8
Hf $4f_{7/2}$	17.0	2.0	16.6	1.8
Hf $4f_{5/2}$	18.7	1.6	18.2	1.7
Hf^{x+} (suboxides)	15.8	3.2	15.6	2.9
Hf^{0} (metal, bulk)	-	-	12.6	2.9

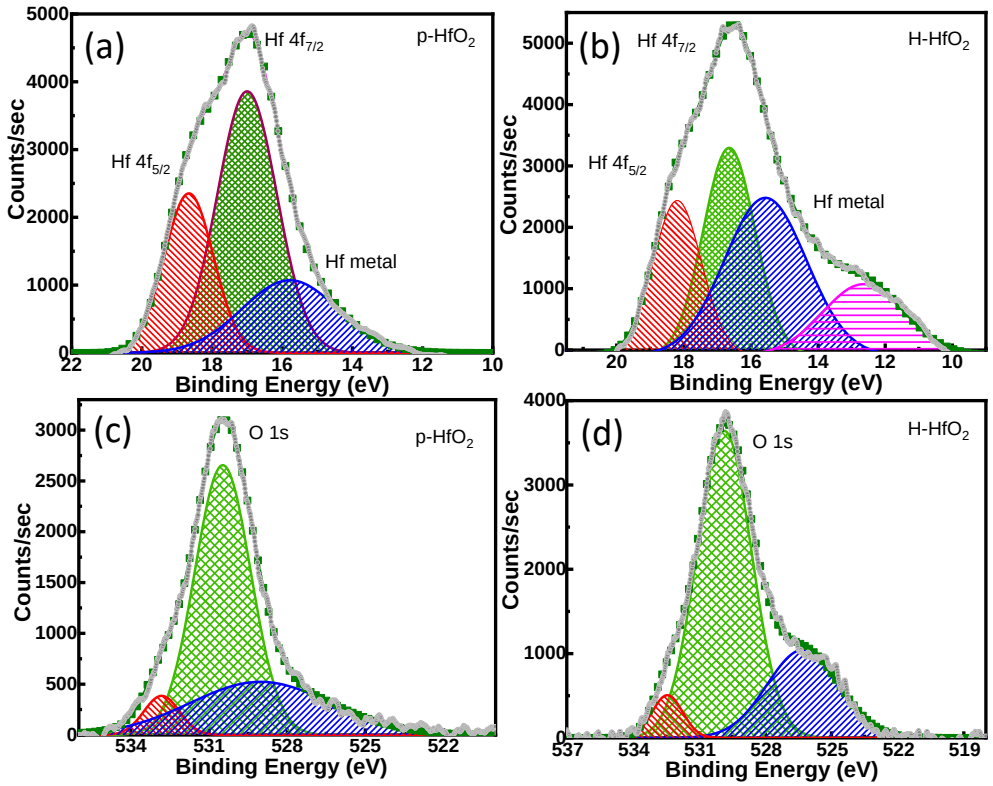

Figure 4.5: X-ray photoelectron spectra (XPS) of Hf 4f and O 1s in (a, c) pristine and (b, d) hydrogenated HfO_2, respectively. The background subtracted raw experimental data is deconvoluted for identifying the peak contributions of Hf metal and suboxides.

Table 4.4: Surface oxygen species present in p-HfO_2, H-HfO_2_6h where $O_{\alpha 2}$, $O_{\alpha 1}$ and O_{β} % are calculated from % area under respective peaks.

Sample	*$O_{\alpha 2}$ (%)*	*$O_{\alpha 1}$ (%)*	*O_{β} (%)*	*$O_{\alpha 1}/O_{\beta}$*
p-HfO_2	5.8	63.1	31.1	2.0
H-HfO_2_6h	5.3	68.7	25.9	2.6

The presence of a peak at binding energies of 16.64 and 16.99 eV for the Hf $4f_{7/2}$ levels has been suggested as Hf^{2+} from HfO.(Lin and Liao 2013) The observed chemical shift in hydrogenated-HfO_2 can be attributed to the removal of oxygen species during hydrogen annealing, creating a change in the bonding environment. Thus, it can be inferred that the Hf 4f

in H-HfO_2 must have partially reduced ions of Hf, which could increase the redox activity and the catalytic activity because of its mixed oxidation states. Peaks occurring at 15.78 and 15.56 eV can be correlated to the presence of suboxide species.(Suzer, Sayan et al. 2003) These values are nearly in accordance with the reported values in the literature.(Barreca, Milanov et al. 2007) The O 1s core level peak showed shifting in the binding energy for the air and hydrogen annealed HfO_2 nanoparticle (Figure 4.5c, d). Each of the peaks is split into three peaks by means of Gaussian peak fitting. The O 1s spectra can be identified with features of chemisorbed oxygen (O_α) and lattice oxygen (O_β) species. The oxygen species present corresponding to binding energies 530.47-529.85 eV can be attributed to the adsorbed surface oxygen or defect oxygen species on the oxygen vacancies ($O_{\alpha1}$), while the binding energies at 532.81-532.43 eV can be ascribed to the adsorbed oxygen species from the hydroxyl group and adsorbed molecular water species ($O_{\alpha2}$).(Fan, Xi et al. 2017) On the other hand, the oxygen species present at the lower binding energies of 529.02−526.28 eV is credited to the presence of lattice oxygen (O_β). The amount of surface oxygen present is quantified (Table 4.4) as the ratio of the peak area of $O_{\alpha1}$ and O_β ($O_{\alpha1}/O_\beta$). (Zhang, Niu et al. 2016) It was observed that the hydrogenated HfO_2 has higher $O_{\alpha1}/O_\beta$ than air annealed HfO_2 by a value of 0.61. Thus, it can be confirmed that even though the air annealed HfO_2 has higher lattice oxygen species present, the hydrogenated HfO_2 overall has higher surface adsorbed oxygen species and therefore might be a beneficial catalyst for exploring soot oxidation activity.

4.2.5 O_2 Temperature-Programmed Desorption (O_2-TPD)

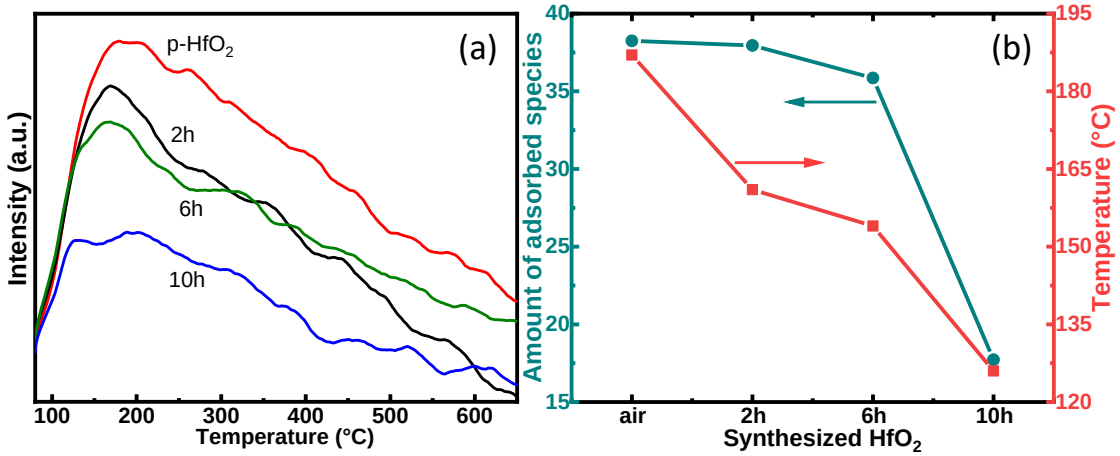

Figure 4.6: O_2-TPD profile and (b) desorption peak temperature for adsorbed oxygen calculated from peak for HfO_2 nanoaggregate samples.

The O_2 TPD measurement was done to further investigate the oxygen species in the pristine and hydrogenated HfO_2 as shown in Figure 4.6a. According to the literature reports, the oxygen species desorbed at a temperature less than 300 °C can be categorized as O_α; these are active surface adsorbed species and corroborate well with the XPS result. Meanwhile, peaks appearing after 300 °C can be assigned to lattice oxygen (O_β) desorption and are ascribed to the release of oxygen from the lattice in oxide material.(Liang, Wu et al. 2008, Fu, Yue et al. 2010) The absence of O_β is understandable, as the lattice oxygen in HfO_2 is not mobile enough to participate in the oxidation process. Broad peaks are observed at temperatures less than 120−190 °C, corresponding to the surface-active oxygen (O^{2-} and O^-) species as a result of chemical adsorption.

Table 4.5. O_2-TPD parameters of the synthesized catalysts

Sl. No.	*Sample*	*Temperature Desorption (°C)*	*Quantity (mmol/g)*	*Amount of adsorbed species (%)*
1.	p-HfO_2	187.7	2.62	38.25
2.	H-HfO_2_2h	161.4	1.17	37.95
3.	H-HfO_2_6h	154.7	1.27	35.86

4.	H-HfO_2_10h	126.8	0.26	17.72

These are the main reactive species in the catalytic oxidation reaction because of its labile nature. (Jampaiah, Velisoju et al. 2017, Li, Du et al. 2017) The detailed parameters of the study are given in Table 4.5. Hydrogenated HfO_2 results in a decrease in the amount of adsorbed species (as seen by the decrease in peak area) with a drop in desorption temperature as shown in Figure 4.6b. The drop in desorption temperature follows a similar trend as that of the increase in lattice strain (Figure 4.2d) in H-HfO_2 nanoaggregates which suggests that lattice strain caused by hydrogenation changes the surface and binding behaviour in the synthesized samples.

4.2.6 Activity Test: Soot Oxidation Activity.

A comparison weight loss curve of pristine and hydrogenated HfO_2 nanoaggregates is shown in Figure 4.7d. The weight change profile shows a decrease in slope below 100 °C, which can be attributed to the decomposition of water and other organics. This step is followed by saturation (only ~1% decrease), leaving the mass of the original HfO_2 nearly constant, which indicates the stability of HfO_2 over a wide range of temperatures. The as-synthesized p-HfO_2 and H-HfO_2 samples were used for analyzing the soot oxidation activity because of its fine particle size and highly porous structure. The soot oxidation is tested under zero air (21% O_2 in N_2).

Table 4.6. TGA parameters of the as synthesized HfO_2 and after accelerated thermal test (ATT)

Sl. No.	Samples	T_m (in °C)		T_{10} (in °C)		T_{50} (in °C)		T_{90} (in °C)	
		As synthesized	After ATT	As synthesized	After ATT	As synthesized	After ATT	As synthesized	After ATT
1.	p-HfO_2	658	705	481	448	644	692	706	761
2.	H-HfO_2_2h	636	722	551	296	632	707	686	774
3.	H-HfO_2_6h	649	704	580	571	646	690	698	751
4.	H-HfO_2_10h	663	724	576	217	649	711	707	780
5.	Carbon	748	-	699	-	745	-	782	-

Figure 4.1b is a schematic representation of the process for analyzing the soot oxidation activity. Briefly, the soot is mixed with the synthesized catalyst and then put in a TGA with an O_2 gas inlet. The soot oxidation profile in terms of percentage weight loss curve against temperature (in °C) is shown in Figure 4.7a. The light-off temperature at which 50% of the total weight loss occurs (T_{50}), and the temperature at the inflection point (T_m) obtained from the derivative curve are used to study the temperature of maximal soot conversion rate where the CO_2 is maximum. (Aneggi, de Leitenburg et al. 2006) The T_{50} for bare soot (carbon black) oxidation without a catalyst is 746 °C (Figure 4.7d). After the inclusion of catalysts, the temperature for 50% conversion is decreased to 644 °C for air annealed p-HfO_2 which further decreases for the hydrogenated HfO_2 to 632 °C for H-HfO_2_2h. Thus, it can be deduced that the presence of the HfO_2 catalyst accelerates the soot oxidation activity. Without the use of the catalyst, the onset temperature (T_{10}), at which 10% soot conversion takes place, is 699 °C, which is reduced to a range of (481−580 °C) in the presence of the HfO_2 (Table 4.6 and Figure 4.7b). The presence of HfO_2 decreases T by about (96−113) °C. Among all of the screened catalysts, p-HfO_2 showed the minimum T_{10} activity at 481 °C, while H-HfO_2_2h showed good catalytic performance, in which the T_{10} and T_{50} decrease by 148 and 113 °C, respectively. Thus, the soot conversion under the tight contact mode and in the presence of catalysts according to the T10 activity followed the trend p-HfO_2 < H_HfO_2_2h < H_HfO_2_10h < H_HfO_2_6h (Figure 4.7a). Catalyst incorporated soot oxidation experiments revealed that the T_m values decrease in chronological order: 663, 658, 649, and 636 °C for H-HfO_2_10h, p-HfO_2, H-HfO_2_6h, and H-HfO_2_2h, respectively.

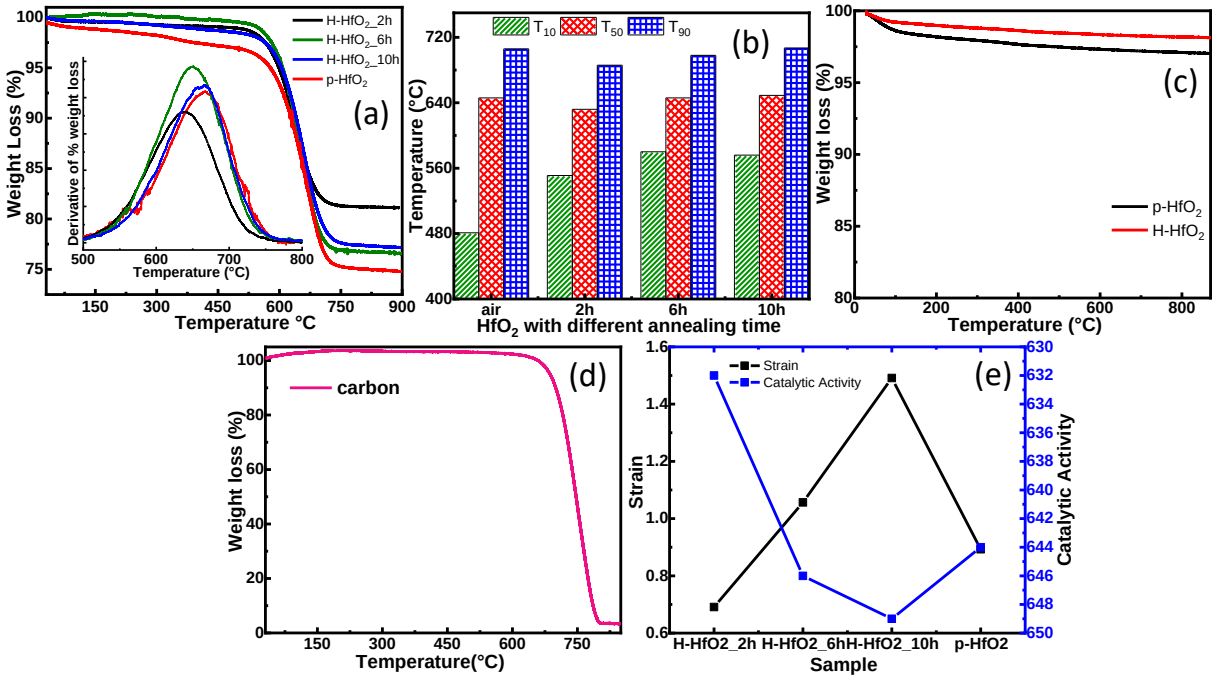

Figure 4.7: (a) TGA profiles of carbon soot/HfO_2 mixtures (catalyst/soot ratio of 4:1) of different HfO_2 samples annealed in air and hydrogen, % weight loss curve and inset is the derivative of weight loss function indicating oxidative peak profile. (b) Bar graph showing the T10, T50, and T90 temperatures in (°C) for all of the prepared samples; the values are indicated in Table 4.5. (c) Thermogravimetric analysis of pristine and hydrogenated HfO_2. (d) TGA data showing the weight loss curve of carbon with T_{50} at 746 °C. (e) Plot of Strain and catalytic activity of the synthesized nanomaterials.

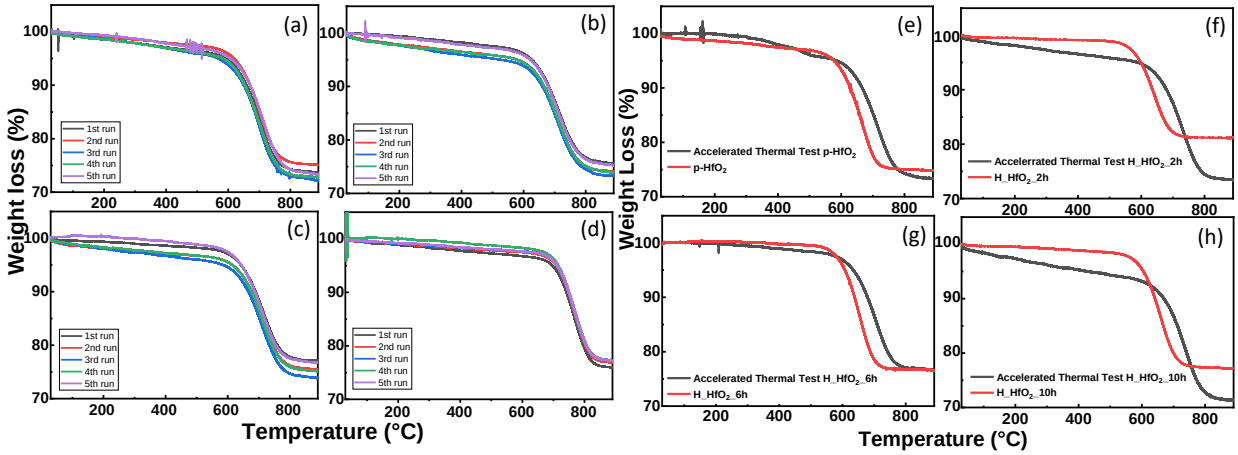

Figure 4.8: Reusability test of the synthesized nanomaterials as the catalyst, TGA plot of the as synthesized samples of HfO_2 with and without an accelerated thermal test.

Although the onset temperature (T_{10}) is lowest for p-HfO_2, the peak temperature (T_m), light-off temperature (T_{50}), and the maximal conversion temperature (T_{90}) are lowest for the 2 h hydrogen annealed HfO_2. The good performance is attributed to higher surface adsorbed oxygen in the case of hydrogenated HfO_2 (as described above in Chemical Analysis). The active oxygen present for the soot conversion activity highly depends on the number of oxygen vacancies created upon the surface of the oxide material used.(Fino, Bensaid et al. 2016) Consequently, the chemisorbed oxygen due to the surface adsorbed oxygen species present on the oxygen vacant sites contributed remarkably during the soot oxidation, which agrees well with the XPS and O_2-TPD results as well. The durability of the catalyst is further tested by performing an accelerated thermal test. The catalyst is heated at 850 °C under humidified N_2 for 2 h followed by an oxidation cycle. The results are shown in Figure 4.8a-d and Table 4.6. The catalyst has been tested for five cycles and showed little loss of catalytic activity (Figure 4.8d-h). Future studies will involve testing the optimized catalyst with other gaseous species such as

H_2O, CO_x, NO_x, and hydrocarbons to understand the applicability of the catalyst in real conditions.

4.3 Conclusion

Although many innovative designs of materials for soot oxidation have been proposed over the years, it is the first for HfO_2 to be used as a catalytic material. Herein, this study, efforts to demonstrate a facile method for synthesizing HfO_2 nanoaggregates, the textural and structural properties of which can be changed by hydrogen annealing. Analysis using various techniques revealed the effect of hydrogen annealing, which was identified to cause increased lattice strain and visible expansion of the nanoaggregates in the TEM images, giving rise to its porous nature and strongly affecting the surface and binding of adsorbates, which was further confirmed by BET. In addition, XPS and O_2-TPD analysis observed a higher percentage of surface adsorbed oxygen compared to the lattice oxygen present, prompting good catalytic soot oxidation activity. This adsorbed surface oxygen desorbed at lower temperatures showed the labile nature of the active oxygen species involved during the oxidation reaction. Moreover, hydrogenation created higher oxygen vacant sites, increasing the possible generation of active oxygen species and the possibility to gain oxygen form the bulk of the materials and other gaseous sources. Thus, inert and stable HfO_2 nanomaterial can be effectively optimized by tuning its properties at lower temperature under a reducing atmosphere. These nanomaterials can be further probed for properties like electrical and optical properties for use in various devices.

...